



OPEN Multi-sequence magnetic resonance imaging radiomics combined with imaging features predicts the difficulty of HIFU treatment of uterine fibroids

Li Shen^{1,4}, Xiao Huang^{1,4}, Yuyao Liu¹, Shanwei Bai², Fang Wang³ & Quan Yang¹✉

To establish a multivariate linear regression model for predicting the difficulty of high-intensity focused ultrasound (HIFU) ablation of uterine fibroids based on multi-sequence magnetic resonance imaging radiomics features. A retrospective analysis was conducted on 218 patients with uterine fibroids who underwent HIFU treatment, including 178 cases from Yongchuan Hospital of Chongqing Medical University and 40 cases from the Second Affiliated Hospital of Chongqing Medical University (external validation set). Radiomics features were extracted and selected from magnetic resonance images, and potentially related imaging features were collected. The energy efficiency factor (EEF) was used as the dependent variable. Imaging models, radiomics models, and joint models were established using a stepwise approach. The model with the highest R^2 value was selected for external validation. The R^2 value of the combined model was 0.642, higher than that of other models. Spearman correlation analysis showed a correlation coefficient of $R = 0.824$ ($P < 0.001$) between predicted EEF and actual EEF. External validation yielded a correlation coefficient of $R = 0.645$ ($P < 0.001$). A model for predicting EEF has been developed, which is clinically important for predicting the difficulty of HIFU treatment of uterine fibroids.

Keywords Uterine fibroids, HIFU, EEF, Radiomics

Uterine fibroids are the most common benign tumor of the female reproductive system. Treatment options for fibroids include surgery, medications, and other treatments, each with its own advantages and disadvantages^{1,2}. The demand for non-invasive treatment techniques is increasing as living standards improve and therapeutic measures are optimized. High-intensity focused ultrasound (HIFU) is a therapeutic method that concentrates ultrasound energy in the target area, creating instantaneous high temperatures and causing coagulative necrosis of fibroid tissue^{3,4}. HIFU has been widely chosen by patients with fertility needs or who require uterine preservation, and has been proven to be very safe and effective⁵. However, not all patients with uterine fibroids are suitable for HIFU treatment, and how to select suitable patients is a clinical concern. Energy efficiency factor (EEF) refers to the ultrasound energy required to ablate a unit volume, which is a key index to quantify the difficulty of ablation, and the EEF value is negatively correlated with the difficulty of ablation. Previous studies have established linear regression models to predict the EEF based on magnetic resonance imaging features^{6,7}. However, the imaging features of magnetic resonance are often measured subjectively, whereas radiomics can convert medical images into high-dimensional quantitative information to capture the potential heterogeneity of uterine fibroids⁸. There are a few studies that use radiomics features for predicting EEF^{9,10}. In this study, based on the multisequence magnetic resonance radiomics features and imaging features, the imaging model, the radiomics model, and the joint model were established and compared, and then a better multiple linear regression model for predicting the ease of ablation of uterine fibroids with HIFU was obtained.

¹Yongchuan Hospital of Chongqing Medical University, Chongqing 402160, China. ²The Second Affiliated Hospital of Chongqing Medical University, Chongqing 400010, China. ³Department of Research and Development, Shanghai United Imaging Intelligence Co., Ltd, Shanghai 200000, China. ⁴These authors contributed equally: Li Shen and Xiao Huang. ✉email: 2644738456@qq.com

Materials and methods

This retrospective study was jointly approved by the Clinical Research Ethics Committee of Yongchuan Hospital of Chongqing Medical University (IRB No. 2024LLS005) and the Ethics Committee of the Second Affiliated Hospital of Chongqing Medical University (No. 2024-41) waived the informed consent. The study strictly followed the Declaration of Helsinki.

Objects of study

A retrospective analysis was conducted on 178 patients from our hospital and 40 patients from an external hospital who underwent HIFU treatment for uterine fibroids between January 2021 and April 2024. 178 patients from our hospital were used to build the model, and 40 patients from outside hospitals were used as an external validation. The average ages of the patients were 45.1 ± 6.4 years (ranging from 23 to 59 years) and 38.3 ± 6.9 years (ranging from 22 to 53 years), respectively.

Inclusion and exclusion criteria

Inclusion Criteria:

- (1) Non-menopausal women over 18 years old;
- (2) Patients have their first pelvic MRI within a week prior to treatment; the second pelvic MRI is performed 2–3 days after treatment.
- (3) No treatment was performed prior to the MR examination;
- (4) MR images are of good quality and allow for region of interest outlining.

Exclusion criteria:

- (1) Patients with all uterine fibroids measuring less than 1 cm in length will be excluded. (I.e., a patient will only be excluded if all fibroids in their body are less than 1 cm in length. If there is at least one fibroid that is larger than or equal to 1 cm, the patient will not be excluded.);
- (2) Pregnant or planning for pregnancy during HIFU treatment;
- (3) Presence of other pelvic diseases;
- (4) Contraindications for MRI examination.

HIFU ablation procedure

All patients were treated in the prone position with their lower abdomen in full contact with a degassed water-filled cushion to ensure effective transmission of ultrasonic energy. The ablation process was performed under sedation and analgesia to alleviate patient discomfort. The irradiation site, duration, and interval were adjusted based on the patient's real-time treatment feedback and clinical tolerance. During treatment, the JC-200D ultrasound-guided HIFU system produced by Chongqing Haifu Medical Technology Co., Ltd. was used, equipped with a concave self-focusing transducer with a focal length of 12.2 cm, a diameter of 20.0 cm, and an operating frequency of 0.9 MHz. The power was adjustable between 40 and 400W, with precise movement of the treatment area achieved through a computer-controlled motion device. A B-mode ultrasound diagnostic probe (Mindray DC-805, 3.5 MHz) located at the center of the transducer was used for real-time guidance and monitoring of the treatment process, ensuring treatment accuracy and safety. After treatment, a professional doctor with at least five years of experience in ultrasound ablation assessed the ablation status of the fibroids based on changes in grayscale on the ultrasound images and decided whether to continue or terminate treatment. The entire treatment process was closely monitored to ensure patient safety and treatment effectiveness.

Instruments and methods

Magnetic resonance examination techniques

All patients underwent pelvic MR examination before and after treatment, including T2-weighted imaging fat suppression (T2WI-FS), contrast-enhanced T1WI (CE-T1WI) and diffusion weighted imaging (DWI). Siemens Verio dot 3.0 T MR was used in our patients, and the scanning parameters are shown in Table 1. The Siemens Prisma 3.0 T and Siemens Avanto 1.5 T MRI devices were used for patient examinations at a single external hospital we collaborated with, with scanning parameters shown in Table 2.

General information

Two experienced abdominal imaging diagnostic radiologists analyzed and measured the following parameters from the MRI images: age, shortest distance from the ventral side to the skin at the level of the center of the target fibroid, thickness of the abdominal wall at the level of the center of the target fibroid, thickness of the

Sequences	Flip angle (deg)	TR (ms)	TE (ms)	Slice thickness (mm)	Spacing between slices (%)	NEX (Number of Excitations)	Acquisition duration (s)	FOV (mm ²)	Acquisition matrix
T2WI-FS	150	3430	85	5	20	1	164	240 × 240	256 × 256
CE-T1WI	9	3	1	4	20	1	24	325 × 400	260 × 320
DWI	–	4600	68	5	20	4	190	230 × 230	140 × 140

Table 1. Main parameters of each sequence of MRI in Yongchuan Hospital of Chongqing Medical University.

Sequences	Flip angle (deg)	TR (ms)	TE (ms)	Slice thickness (mm)	Spacing between slices	NEX (Number of Excitations)	Acquisition duration (s)	FOV (mm ²)	Acquisition matrix
T2WI-FS	160, 160	3600, 4000	90, 105	4, 5	25%, 25%	1, 1	107, 60	320 × 320, 315 × 300	320 × 272, 256 × 205
CE-T1WI	9, 12	3.3, 4.7	1.3, 1.6	2, 4	20%, 20%	1, 1	119, 135	380 × 380, 320 × 320	320 × 240, 320 × 288
DWI	–, –	4400, 5200	53, 72	4, 5	25%, 20%	4, 3	97, 78	300 × 234, 350 × 285	164 × 164, 150 × 123

Table 2. Main parameters of each sequence of MRI in the Second Affiliated Hospital of Chongqing Medical University. 3.0 T before comma, 1.5 T after comma.

subcutaneous fat, distance from the dorsal side of the uterine fibroid to the sacrum, volume of uterine fibroid¹¹ ($V = \pi/6 \times \text{upper and lower diameter} \times \text{left and right diameter} \times \text{anterior and posterior diameter}$), non-perfused volume (NPV, NPV is the necrotic volume of fibroids, measured on enhanced images. $^{11}V' = \pi/6 \times \text{upper and lower diameters}' \times \text{left and right diameters}' \times \text{anterior and posterior diameters}'$) T2WI signal (measured at the fibroid center level and two levels above and below it for a total of 3 levels and averaged), uterine position, type of fibroid, degree of enhancement on T1WI (below myometrium = mild enhancement, similar to myometrium = moderate enhancement, higher than myometrium = significant enhancement), DWI signal intensity (compared to the myometrium, low signal = hypointense, similar to the myometrium = isointense, high signal = hyperintense).

The following metrics were collected from the patients' clinical cases: average irradiation power (W), irradiation time (s, the time taken to irradiate the target fibroid). The EEF was calculated, $EEF^{11} = \eta \times P \times t/V'$ (J/mm^3), where η represents the focusing coefficient of the HIFU transducer, quantifying its ability to concentrate ultrasonic energy in the focal region ($\eta = 0.7$). P denotes the ultrasound power (W), and t denotes the irradiation time.

Radiomics features

Two radiologists delineated the region of interest (ROI) using the Uniportal AI Research Portal (V730) software¹². Layer-by-layer segmentation was performed throughout the entire fibroid using preoperative T2WI-FS, CE-T1WI, and DWI sequences. To avoid the influence of volume effects, images with unclear edge contours were discarded (specifically, peripheral vessels or large vessels were not included in the ROI), and radiomics features were extracted solely from the delineated ROI. To assess the repeatability of radiomics features, images of 50 randomly selected patients were re-segmented by the two radiologists one month later. The interclass correlation coefficients (ICC) were used to evaluate the consistency of each index. An ICC > 0.75 was considered to indicate good consistency. The feature data were preprocessed using Z-score normalization, and then the minimum redundancy and maximum correlation (MRMR)¹³ method and the least absolute shrinkage and selection operator (LASSO) were used for feature selection. For a detailed explanation, see Supplement file 1.

Statistical analysis

SPSS 26.0 statistical analysis software was used, the normality of the data was examined through assessments of skewness and kurtosis coefficients, and measures that conformed to normal distribution were expressed as mean ± standard deviation; measures that did not conform to normal distribution were expressed as the median and the interquartile range. Define separate dummy variables for multicategorical variables. EEF was used as the dependent variable and the possible influencing factors as independent variables, and multiple linear regression models were established using stepwise regression (the criteria for introduction and elimination were $p < 0.05$ and $p \geq 0.10$, respectively). The superiority of the models was evaluated by the coefficient of determination (R^2 , $0 \leq R^2 \leq 1$) and the adjusted R^2 , with larger values indicating a better model fit. The Durbin-Watson test was used to evaluate whether the residuals of the regression models were independent or not (the range of values was 0 ~ 4), and when the Durbin-Watson value was close to 2, it indicated that the residuals were independent and the model was established. ANOVA was performed on all models, where $p < 0.05$ indicates statistical significance. Additionally, multicollinearity diagnosis was conducted based on tolerance and variance inflation factor (VIF), with tolerance < 0.1 or VIF > 10 indicating multicollinearity among independent variables.

Results

General information on uterine fibroids

The general characteristics of uterine fibroids are shown in Tables 3 and 4 below. Bivariate correlation analysis of the different independent variables with the dependent variable EEF in our institution yielded the following: shortest distance from the ventral side to the skin at the level of the center of the target fibroid, thickness of the abdominal wall at the level of the center of the target fibroid, thickness of the subcutaneous fat, distance from the dorsal side of the uterine fibroid to the sacrum, volume of uterine fibroid, T2WI signal, uterine position, type of fibroid, degree of enhancement on T1WI were statistically significant ($p < 0.05$). The remaining imaging features were not found to be statistically significant.

Radiomics features

For each case, 2231 (T2WI-FS sequences), 2227 (CE-T1WI sequences), and 2199 (DWI sequences) radiomics features with ICC > 0.75 were extracted. After MRMR and LASSO screening, 8 T2WI-FS features, 8 CE-T1WI

Characteristics	EEF		
	Value	P	The kind of test-statistic
Number of patients (n)	178	–	–
Age (y)	45.1 ± 6.4	0.322	Spearman
Shortest distance from the ventral side to the skin at the level of the center of the target fibroid (mm)	52.9 ± 24.1	< 0.001	Spearman
Thickness of the abdominal wall at the level of the center of the target fibroid (mm)	28.7 ± 8.4	0.007	Spearman
Thickness of the subcutaneous fat (mm)	20.2 ± 7.9	0.009	Spearman
Distance from the dorsal side of the uterine fibroid to the sacrum (mm)	26.6 (12.4, 43.8)	0.023	Spearman
Volume of uterine fibroid (mm ³)	62668.8 (20554.8, 141001.7)	< 0.001	Spearman
NPV (mm ³)	44934.4 (15523.5, 104459.7)	< 0.001	Spearman
T2WI signal	182.0 ± 80.0	0.027	Spearman
Uterine position (anterior/medial/posterior)	103/28/47 (57.9%/15.7%/26.4%)	0.023	H-test
Type of fibroid (intermural/submucosal/subserosal)	154/9/15 (86.5%/5.1%/8.4%)	0.007	H-test
Degree of enhancement on T1WI (mild/moderate/significant)	81/40/57 (45.5%/22.5%/32%)	0.013	H-test
DWI signal intensity (hypointense /isointense/hyperintense)	77/46/55 (43.3%/25.8%/30.9%)	0.792	H-test
Average irradiation power (W)	400 (391.5, 400)	0.265	Spearman
Irradiation time (s)	542 (330.5, 882.5)	0.559	Spearman
EEF (J/mm ³)	3.4 (1.9, 7.2)	–	–

Table 3. General characteristics of uterine fibroids in our institution.

Characteristics	EEF		
	Value	P	The kind of test-statistic
Number of patients (n)	40	–	–
Age (y)	38.3 ± 6.9	0.451	Spearman
Shortest distance from the ventral side to the skin at the level of the center of the target fibroid (mm)	52.3 ± 22.1	0.015	Spearman
Thickness of the abdominal wall at the level of the center of the target fibroid (mm)	26.9 ± 7.7	0.507	Spearman
Thickness of the subcutaneous fat (mm)	20.7 ± 6.6	0.774	Spearman
Distance from the dorsal side of the uterine fibroid to the sacrum (mm)	19.7 (9.1, 43.1)	0.936	Spearman
Volume of uterine fibroid (mm ³)	99615.5 (63524.3, 143242.4)	0.001	Spearman
NPV (mm ³)	92768.4 (62866.0, 133006.6)	< 0.001	Spearman
T2WI signal	218.8 ± 104.4	0.036	Spearman
Uterine position (anterior/medial/posterior)	29/3/8 (72.5%/7.5%/20.0%)	0.319	H-test
Type of fibroid (intermural/submucosal/subserosal)	30/5/5 (75.0%/12.5%/12.5%)	0.001	H-test
Degree of enhancement on T1WI (mild/moderate/significant)	17/10/13 (42.5%/25.0%/32.5%)	0.995	H-test
DWI signal intensity (hypointense /isointense/hyperintense)	18/6/16 (45.0%/15.0%/40.0%)	0.042	H-test
Average irradiation power (W)	400 (400, 400)	0.578	Spearman
Irradiation time (s)	790.0 (541.0, 1150.3)	0.620	Spearman
EEF (J/mm ³)	2.5 (1.7, 3.7)	–	–

Table 4. General Characteristics of Uterine Fibroids from a Single External Hospital We Collaborated With.

features and 7 DWI features were retained, respectively (Table 5, Supplementary table 1 and Supplementary file 2).

Model establishment

Construction of multiple linear regression model for EEF based on imaging features

The nine statistically significant imaging features mentioned above were used as independent variables, and EEF was used as the dependent variable to establish a multiple linear regression model, and the regression analysis was performed using the “stepwise method”. The final linear regression model sequentially incorporated the following five statistically significant imaging features: volume of uterine fibroid, shortest distance from the ventral side to the skin at the level of the center of the target fibroid, submucosal fibroid, significant enhancement of T1WI, distance from the dorsal side of the uterine fibroid to the sacrum (Table 6).

The final EEF regression model had an R^2 of 0.384 and an adjusted R^2 of 0.367. ANOVA showed $F = 21.485$, $P < 0.001$, indicating that all models were statistically significant ($p < 0.001$). The Durbin-Watson value was 2.038, close to the standard value of 2, indicating independent residuals and model validity. Collinearity tests showed that all variables had a tolerance greater than 0.1 and VIF < 10, indicating no collinearity issues

Characteristics	Value
T2-log_gldm_log-sigma-1-0-mm-3D-SmallDependenceLowGrayLevelEmphasis	0.001 (0.001, 0.002)
T2-log_ngtdm_log-sigma-2-0-mm-3D-Busyness	11.315 (6.504, 23.626)
T2-wavelet_grlm_wavelet-LHL-GrayLevelNonUniformity	1768.353 (740.203, 3691.349)
T2-wavelet_grlm_wavelet-HHL-LongRunLowGrayLevelEmphasis	0.655 (0.390, 0.803)
T2-normalize_gldm_SmallDependenceLowGrayLevelEmphasis	0.005 (0.004, 0.006)
T2-discretegaussian_glszm_GrayLevelNonUniformity	23.074 (12.433, 45.121)
T2-specklenoise_glcm_Imc1	-0.031 (-0.069, -0.017)
T2-shotnoise_glcm_Id	0.524 (0.483, 0.563)
A1-additivegaussiannoise_ngtdm_Busyness	4.703 (2.560, 8.691)
A1-log_ngtdm_log-sigma-0-5-mm-3D-Busyness	144.713 (64.536, 283.484)
A1-log_ngtdm_log-sigma-0-5-mm-3D-Coarseness	0.000 (0.000, 0.001)
A1-wavelet_glcm_wavelet-LLH-Idmn	0.997 (0.995, 0.998)
A1-wavelet_grlm_wavelet-LHH-ShortRunEmphasis	0.564 (0.548, 0.590)
A1-wavelet_grlm_wavelet-HHH-RunEntropy	2.806 (2.753, 2.839)
A1-normalize_glcm_ClusterTendency	0.647 (0.489, 0.774)
A1-mean_ngtdm_Strength	0.115 (0.065, 0.218)
DWI-binomialblurimage_glszm_LargeAreaEmphasis	134528.036 (36108.285, 450965.272)
DWI-log_grlm_log-sigma-1-0-mm-3D-RunPercentage	0.586 (0.560, 0.622)
DWI-log_ngtdm_log-sigma-1-0-mm-3D-Coarseness	0.002 (0.001, 0.005)
DWI-wavelet_glcm_wavelet-HHH-Correlation	-0.026 (-0.029, -0.024)
DWI-wavelet_glszm_wavelet-HLH-LargeAreaHighGrayLevelEmphasis	1099810.044 (210152.726, 4137022.818)
DWI-wavelet_gldm_wavelet-LHH-SmallDependenceLowGrayLevelEmphasis	0.003 (0.002, 0.006)
DWI-normalize_glszm_GrayLevelNonUniformity	10.386 (4.333, 19.095)

Table 5. List of the 23 radiomics parameters screened. T2 denotes image histologic features extracted based on T2WI-FS sequences; A1 denotes image histologic features extracted based on CE-T1WI sequences; DWI denotes image histologic features extracted based on DWI sequences. For specific feature definitions and explanations, please refer to the Pyradiomics website: <https://pyradiomics.readthedocs.io/en/latest/index.html>.

model	R	R ²	Adjusted R ²	F	P	Durbin watson
1	0.401 ^a	0.161	0.156	33.714	0.000 ^a	
2	0.492 ^b	0.242	0.233	27.955	0.000 ^b	
3	0.565 ^c	0.320	0.308	27.258	0.000 ^c	
4	0.606 ^d	0.367	0.352	25.089	0.000 ^d	
5	0.620 ^e	0.384	0.367	21.485	0.000 ^e	2.038

Table 6. Multiple linear regression model of EEF based on imaging features. a. Predictor variable: (constant), volume of uterine fibroid. b. Predictor variables: (constants), volume of uterine fibroid, shortest distance from the ventral side to the skin at the level of the center of the target fibroid. c. Predictor variables: (constants), volume of uterine fibroid, shortest distance from the ventral side to the skin at the level of the center of the target fibroid, submucosal fibroid. d. Predictor variables: (constant), volume of uterine fibroid, shortest distance from the ventral side to the skin at the level of the center of the target fibroid, submucosal fibroid, significant enhancement of T1WI. e. Predictor variables: (constant), volume of uterine fibroid, shortest distance from the ventral side to the skin at the level of the center of the target fibroid, submucosal fibroid, significant enhancement of T1WI, distance from the dorsal side of the uterine fibroid to the sacrum. f. Dependent variable: EEF.

among the independent variables. According to Table 7, the multiple linear regression equation is $Y1 = 0.272 - 0.000011X_1 + 0.076X_2 + 6.523X_3 + 2.906X_4 + 0.045X_5$, where X_1 = volume of uterine fibroid, X_2 = shortest distance from the ventral side to the skin at the level of the center of the target fibroid, X_3 = submucosal fibroid, X_4 = significant enhancement of T1WI, and X_5 = distance from the dorsal side of the uterine fibroid to the sacrum.

Construction of EEF multiple linear joint regression model for radiomics features

A multiple linear regression model was constructed with the above 23 radiomics features (8 from T2WI-FS, 8 from CE-T1WI, and 7 from DWI) as the independent variables and EEF as the dependent variable, and the regression analysis was performed using the “stepwise method”, and a total of 7 radiomics features were included in the final linear regression model in the order of the following 7 features: T2- specklenoise_glcm_Imc1, A1-

Model		Unstandardized coefficient		Standardized coefficient	P	covariance diagnosis	
		B	standard error	Beta		tolerances	VIF
5	(Constant)	0.272	1.444		0.851		
	Volume of uterine fibroid	-0.000011	0.000	-0.290	0.000	0.804	1.244
	Shortest distance from the ventral side to the skin at the level of the center of the target fibroid	0.076	0.016	0.315	0.000	0.774	1.291
	Submucosal fibroid	6.523	1.600	0.247	0.000	0.971	1.030
	Significant enhancement of T1WI	2.906	0.757	0.235	0.000	0.957	1.045
	Distance from the dorsal side of the uterine fibroid to the sacrum	0.045	0.021	0.154	0.029	0.730	1.370

Table 7. Multiple linear regression analysis of EEF based on imaging characteristics.

Model	R	R ²	Adjusted R ²	F	P	Durbin Watson
1	0.674 ^a	0.454	0.451	146.255	0.000 ^a	
2	0.710 ^b	0.504	0.498	88.961	0.000 ^b	
3	0.734 ^c	0.539	0.531	67.774	0.000 ^c	
4	0.752 ^d	0.566	0.556	56.427	0.000 ^d	
5	0.767 ^e	0.588	0.576	49.106	0.000 ^e	
6	0.774 ^f	0.599	0.585	42.548	0.000 ^f	
7	0.781 ^g	0.609	0.593	37.858	0.000 ^g	1.745

Table 8. Multiple linear regression model of EEF based on radiomics features. a. Predictor variables: (constants), T2-specklenoise_glcmm_Ic1. b. Predictor variables: (constants), T2-specklenoise_glcmm_Ic1, A1-mean_ngtdm_Strength. c. Predictor variables: (constants), T2-specklenoise_glcmm_Ic1, A1-mean_ngtdm_Strength, DWI-log_ngtdm_log-sigma-1-0-mm-3D-Coarseness. d. Predictor variables: (constants), T2-specklenoise_glcmm_Ic1, A1-mean_ngtdm_Strength, DWI-log_ngtdm_log-sigma-1-0-mm-3D-Coarseness, A1-wavelet_glrmm_wavelet-HHH-RunEntropy. e. Predictor variables: (constants), T2-specklenoise_glcmm_Ic1, A1-mean_ngtdm_Strength, DWI-log_ngtdm_log-sigma-1-0-mm-3D-Coarseness, A1-wavelet_glrmm_wavelet-HHH-RunEntropy, A1-log_ngtdm_log-sigma-0-5-mm-3D-Coarseness. f. Predictor variables: (constants), T2-specklenoise_glcmm_Ic1, A1-mean_ngtdm_Strength, DWI-log_ngtdm_log-sigma-1-0-mm-3D-Coarseness, A1-wavelet_glrmm_wavelet-HHH-RunEntropy, A1-log_ngtdm_log-sigma-0-5-mm-3D-Coarseness, T2-wavelet_glrmm_wavelet-HHL-LongRunLowGrayLevelEmphasis. g. Predictor variables: (constants), T2-specklenoise_glcmm_Ic1, A1-mean_ngtdm_Strength, DWI-log_ngtdm_log-sigma-1-0-mm-3D-Coarseness, A1-wavelet_glrmm_wavelet-HHH-RunEntropy, A1-log_ngtdm_log-sigma-0-5-mm-3D-Coarseness, T2-wavelet_glrmm_wavelet-HHL-LongRunLowGrayLevelEmphasis, A1-log_ngtdm_log-sigma-0-5-mm-3D-Busyness. h. Dependent variable: EEF.

mean_ngtdm_Strength, DWI-log_ngtdm_log-sigma-1-0-mm-3D-Coarseness, A1-wavelet_glrmm_wavelet-HHH-RunEntropy, A1-log_ngtdm_log-sigma-0-5-mm-3D-Coarseness, T2-wavelet_glrmm_wavelet-HHL-LongRunLowGrayLevelEmphasis, A1-log_ngtdm_log-sigma-0-5-mm-3D-Busyness (Table 8).

The final EEF regression model had an R² of 0.609 and an adjusted R² of 0.593. ANOVA showed F = 37.858, P < 0.001, indicating that all models were statistically significant (p < 0.001). The Durbin-Watson value was 1.745, close to the standard value of 2, indicating independent residuals and model validity. Collinearity tests showed that all variables had a tolerance greater than 0.1 and VIF < 10, indicating no collinearity issues among the independent variables. According to Table 9, the multiple linear regression equation is $Y_2 = 87.702 - 63.749X_6 + 5.482X_7 - 240.621X_8 - 29.944X_9 - 932.167X_{10} - 1.164X_{11} - 0.004X_{12}$, where $X_6 =$ T2-specklenoise_glcmm_Ic1; $X_7 =$ A1-mean_ngtdm_Strength; $X_8 =$ DWI-log_ngtdm_log-sigma-1-0-mm-3D-Coarseness; $X_9 =$ A1-wavelet_glrmm_wavelet-HHH-RunEntropy; $X_{10} =$ A1-log_ngtdm_log-sigma-0-5-mm-3D-Coarseness; $X_{11} =$ T2-wavelet_glrmm_wavelet-HHL-LongRunLowGrayLevelEmphasis; $X_{12} =$ A1-log_ngtdm_log-sigma-0-5-mm-3D-Busyness.

Construction of multiple linear joint regression model of EEF based on imaging features and radiomics features.

The above 9 statistically significant imaging features and 23 imaging features were used as independent variables, and the EEF was used as the dependent variable to establish a multiple linear regression model, and the regression analysis was performed using the “stepwise method”, the final linear regression model sequentially incorporated the following six statistically significant characteristics: T2-specklenoise_glcmm_Ic1, submucosal fibroid, A1-mean_ngtdm_Strength, significant enhancement of T1WI, T2-wavelet_glrmm_wavelet-LHL-GrayLevelNonUniformity, DWI-normalize_glszm_GrayLevelNonUniformity (Table 10).

Model		Unstandardized coefficient		Standardized coefficient	P	covariance diagnosis	
		B	standard error	Beta		tolerances	VIF
7	(Constant)	87.702	18.792		0.000		
	T2-specklenoise_glmc_Imc1	-63.749	11.031	-0.636	0.000	0.190	5.266
	A1-mean_ngtdm_Strength	5.482	1.055	0.308	0.000	0.654	1.529
	DWI-log_ngtdm_log-sigma-1-0-mm-3D-Coarseness	-240.621	96.124	-0.302	0.013	0.158	6.311
	A1-wavelet_glrml_wavelet-HHH-RunEntropy	-29.944	6.651	-0.410	0.000	0.277	3.608
	A1-log_ngtdm_log-sigma-0-5-mm-3D-Coarseness	-932.167	281.346	-0.292	0.001	0.295	3.390
	T2-wavelet_glrml_wavelet-HHL-LongRunLowGrayLevelEmphasis	-1.164	0.520	-0.111	0.026	0.938	1.066
A1-log_ngtdm_log-sigma-0-5-mm-3D-Busyness	-0.004	0.002	-0.123	0.035	0.688	1.453	

Table 9. Multiple linear regression analysis of EEF based on radiomics features.

Model	R	R ²	Adjusted R ²	F	P	Durbin Watson
1	0.674 ^a	0.454	0.451	146.255	0.000 ^a	
2	0.716 ^b	0.513	0.507	92.182	0.000 ^b	
3	0.754 ^c	0.568	0.561	76.320	0.000 ^c	
4	0.777 ^d	0.604	0.595	65.892	0.000 ^d	
5	0.795 ^e	0.632	0.622	59.142	0.000 ^e	
6	0.801 ^f	0.642	0.629	51.073	0.000 ^f	1.951

Table 10. Multiple linear regression models of EEF based on imaging features and radiomics features.

a. Predictor variables: (constants), T2-specklenoise_glmc_Imc1. b. Predictor variables: (constant), T2-specklenoise_glmc_Imc1, submucosal fibroid. c. Predictor variables: (constant), T2-specklenoise_glmc_Imc1, submucosal fibroid, A1-mean_ngtdm_Strength. d. Predictor variables: (constant), T2-specklenoise_glmc_Imc1, submucosal fibroid, A1-mean_ngtdm_Strength, significant enhancement of T1WI. e. Predictor variables: (constant), T2-specklenoise_glmc_Imc1, submucosal fibroid, A1-mean_ngtdm_Strength, significant enhancement of T1WI, T2-wavelet_glrml_wavelet-LHL-GrayLevelNonUniformity. f. Predictor variables: (constant), T2-specklenoise_glmc_Imc1, submucosal fibroid, A1-mean_ngtdm_Strength, significant enhancement of T1WI, T2-wavelet_glrml_wavelet-LHL-GrayLevelNonUniformity, DWI-normalize_glszm_GrayLevelNonUniformity. g. Dependent variable: EEF.

Model		Unstandardized coefficient		Standardized coefficient	P	Covariance diagnosis	
		B	standard error	Beta		tolerances	VIF
6	(Constant)	3.144	0.680		0.000		
	T2-specklenoise_glmc_Imc1	-38.269	6.026	-0.382	0.000	0.580	1.725
	Submucosal fibroid	6.560	1.218	0.249	0.000	0.981	1.020
	A1-mean_ngtdm_Strength	4.378	0.924	0.246	0.000	0.777	1.287
	Significant enhancement of T1WI	2.460	0.572	0.199	0.000	0.981	1.020
	T2-wavelet_glrml_wavelet-LHL-GrayLevelNonUniformity	-0.000286	0.000	-0.139	0.025	0.553	1.809
	DWI-normalize_glszm_GrayLevelNonUniformity	-0.057	0.027	-0.129	0.034	0.580	1.723

Table 11. Multiple linear regression analysis of EEF based on imaging features and radiomics features.

The final EEF regression model has an R² of 0.642 and an adjusted R² of 0.629. The analysis of variance shows F = 51.073, with P < 0.001, indicating that all models have statistical significance (p < 0.001). The Durbin-Watson value of the model is 1.951, close to the standard value of 2, indicating independent residuals and a valid model. Collinearity tests show that the tolerance of all variables is greater than 0.1, and VIF < 10, indicating no collinearity issues among the variables. According to Table 11, the multiple linear regression equation is: $Y_3 = 3.144 - 38.269X_6 + 6.560X_3 + 4.378X_7 + 2.460X_4 - 0.000286X_{13} - 0.057X_{14}$, where X_{13} = T2-wavelet_glrml_wavelet-LHL-GrayLevelNonUniformity; X_{14} = DWI-normalize_glszm_GrayLevelNonUniformity.

EEF prediction model efficacy evaluation and validation

The imaging feature prediction model, the radiomics feature prediction model, and the combined model were all statistically significant in explaining the independent variables, and the models were relatively reasonable. The adjusted R² of the combined model (0.629) is the highest, suggesting the best fit. According to the EEF formula,

the calculated actual EEF value is $3.4 (1.9, 7.2) \text{ J/mm}^3$. The relevant data of 178 patients were substituted into the prediction models: Y1, Y2, and Y3, and the predicted EEF values were $6.2 (3.9, 9.3)$, $4.8 (2.3, 7.8)$, and $4.9 (2.4, 7.5) \text{ J/mm}^3$. The correlation between predicted EEF and actual EEF was assessed using Spearman's correlation analysis, with correlation coefficients r of 0.252, 0.781, and 0.824 ($p < 0.001$), respectively, with a better result for predictive model Y3 indicating a highly significant correlation, which was further corroborated by scatterplot analyses showing strong correlation between the two. External validation used 40 patients from an external hospital. The actual EEF values were $2.5 (1.7, 3.7) \text{ J/mm}^3$ and the predicted EEF values were $6.3 (3.5, 10.6)$, $7.4 (6.1, 8.6)$, and $5.1 (3.4, 6.6) \text{ J/mm}^3$ respectively. The correlation coefficients, r , were 0.173, 0.460, and 0.645 ($p < 0.001$), respectively. The results of the predictive model, Y3, were better, which indicated that there was a moderate correlation between the two, and the scatter plot analysis showed that there was a moderate correlation between the two (Fig. 1a, b). Bland-Altman was used to analyse the consistency of the results between the two groups (Fig. 2a, b).

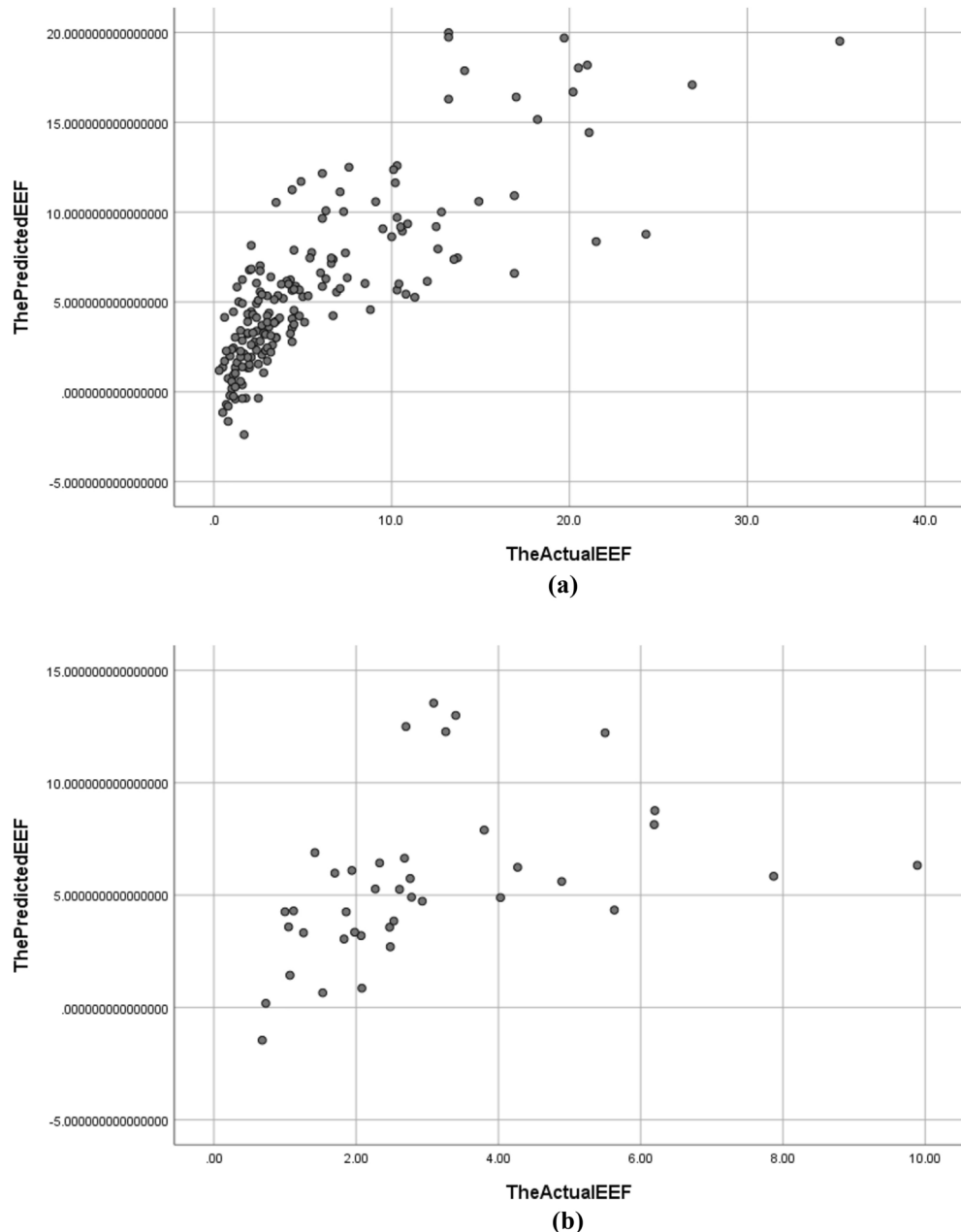


Fig. 1. (a) Scatterplot of EEF values predicted by the final EEF prediction model and actual EEF values (our institution). (b) Scatterplot of EEF values predicted by the final EEF prediction model and actual EEF values (Outer Hospital). *Note* Some predicted EEF values are negative, reflecting the model's extrapolation effect on boundary or extreme data. Negative EEF values hold no actual physical significance and are presented only as reference for the model's prediction characteristics.

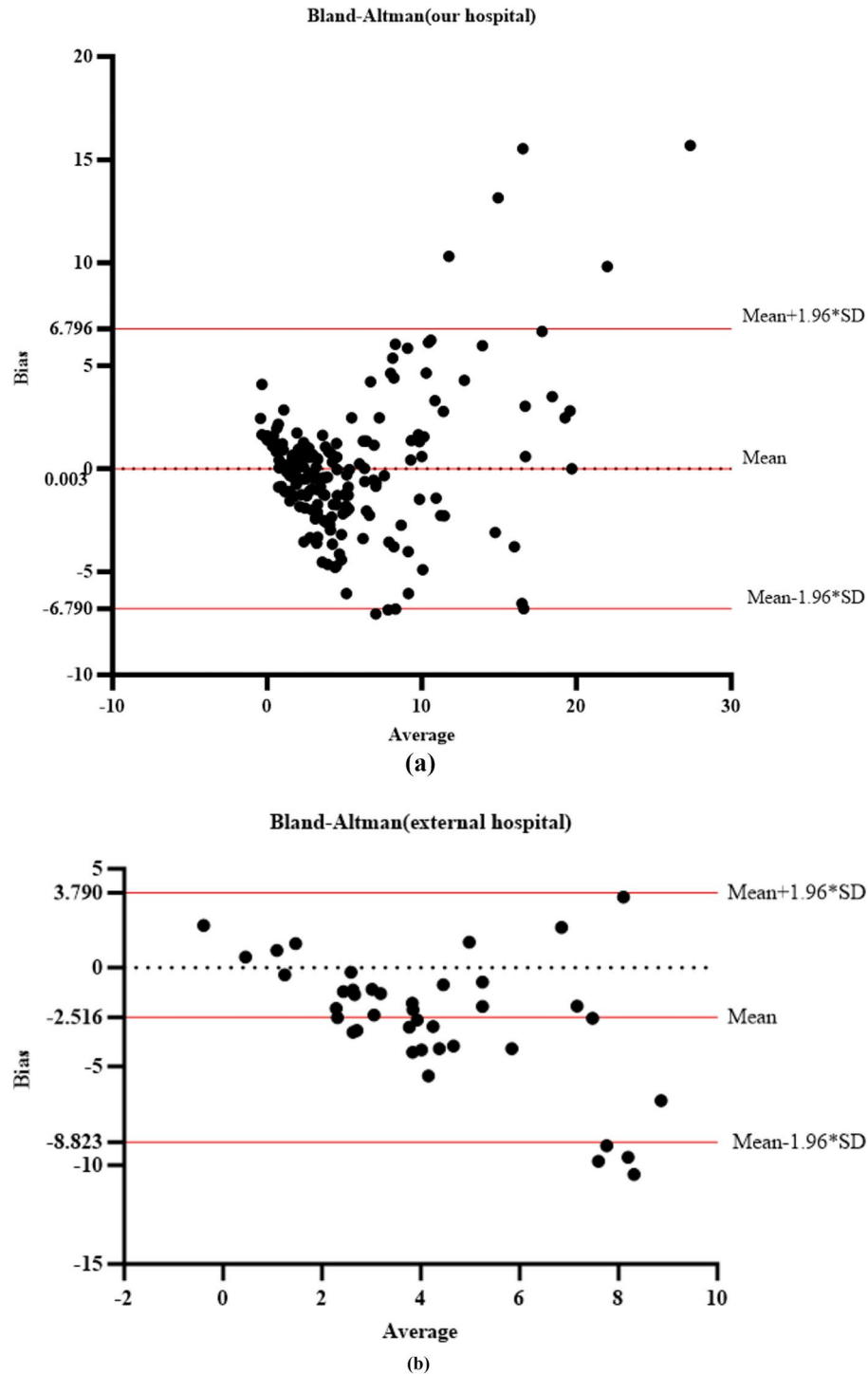


Fig. 2. (a) Bland–Altman (our hospital). (b) Bland–Altman (external hospital).

Discussion

EEF is a key indicator to clinically quantify the dose of HIFU ablation for uterine fibroids and provides valuable insight into the difficulty of HIFU ablation for uterine fibroids. In this study, by establishing an imaging model, a radiomics model, and a combined model, we found that the combined model had the best fit (adjusted $R^2 = 0.629$), which finally incorporated 6 features, namely T2-specklenoise_glmc_Imc1, submucosal fibroid, A1-mean_ngtdm_Strength, Significant enhancement of T1WI, T2-wavelet_glrmlm-wavelet-LHL-GrayLevelNonUniformity, and DWI-normalize_glszm_GrayLevelNonUniformity. quantified the above features and introduced them into the regression model of $EEF.Y_3 = 3.144 - 38.269X_6 + 6.560X_3 + 4.378X_7 + 2.460X_4 - 0.000286X_{13} - 0.057X_{14}$ can be used to calculate the value of EEF.

The first feature that enters the model in this study is T2-specklenoise_glcm_Imc1, which has a biased regression coefficient (B) of -38.269 , negatively affecting the EEF, which is the ability of the texture feature to quantify a certain pattern of grey scale changes or color changes within the region, and previous studies have^{14,15} demonstrated how image results and texture parameters can be linked. Correlation Information Measure 1 (Imc1) assesses the correlation between the probability distributions of and (quantifying the complexity of the texture), this feature is based on T2WI-FS, A larger Imc1 value indicates a more complex texture within the uterine fibroid tissue, which may correspond to greater inhomogeneity in signal intensity. Additionally, a larger Imc1 value accompanied by a smaller EEF value may suggest that fibroids with more complex textures are potentially easier to manage during ablation.

The second feature to enter the model is submucosal fibroid, which is positively correlated with EEF. Submucosal fibroid are more difficult to ablate compared to intermural and subserosal fibroid, probably because ultrasound penetrates more tissue layers resulting in increased attenuation of ultrasound energy; it may also be related to blood supply.

The third and fourth feature to enter the predictive model are A1-mean_ngtdm_Strength and Significant enhancement of T1WI, both of which are obtained based on CE-T1WI and are positively correlated with EEF. Strength is a measure of the primitives in an image, which refers to the basic structures or patterns that are easily defined and visible. Its value is high when the primitives are easily defined and visible, i.e. an image with slow change in intensity but more large coarse differences in gray level intensities. An increase in this value represents an increase in the degree of enhancement, which is consistent with the effect of Significant enhancement on EEF. The higher degree of enhancement on T1WI indicates the richer blood supply of uterine fibroids, and thus the more HIFU ablation energy is taken away by the blood circulation, and the lower the efficiency of energy deposition, so that the ablation is more difficult. Previous related studies^{16,17}, the degree of enhancement on T1WI was entered into the final prediction model, which fully demonstrated that the degree of enhancement on T1WI has an important impact on EEF.

The last two features entering the model are T2-wavelet_glrml_wavelet-LHL-GrayLevelNonUniformity and DWI-normalize_glszm_GrayLevelNonUniformity, obtained based on the T2WI-FS and DWI, respectively, both of which slightly negatively affect EEF ($B = -0.000286$, $B = -0.057$). GrayLevelNonUniformity measures the variability of gray-level intensity values in the image, with a lower value indicating more homogeneity in intensity values. Based on previous studies^{18,19}, we hypothesized that fibroids with a lower value were mainly composed of cellular components, fibroids rich in cell component, due to the difficulty of depositing ultrasound energy and large attenuation of ultrasound energy, resulting in difficulty in heating and ablation; tissue specific perfusion can also affect the peak temperature of fibroid heating.

Yi⁶ et al. and Fan¹¹ et al. established EEF multiple linear regression models based on imaging features, respectively, and the adjusted R^2 of the best model was 0.376 and 0.354. However imaging features are obtained by visual recognition and human measurement, and the error is relatively large. And radiomics can realize the objectivized extraction and quantitative analysis of image features. Wei¹³ Based on the T2WI sequence extraction of radiomics features combined with imaging features to establish a model, the fit of the joint model is better than that of the model based on imaging features, and the adjusted R^2 of the best model is 0.297. In this study, the best model is based on the combination of multiple sequences of radiomics features and imaging features, which can provide the biological information of the uterine fibroids in multiple ways compared with single sequences, and its adjusted R^2 is 0.629, while Spearman correlation analysis yielded that the predicted EEF and the actual EEF are highly correlated ($r = 0.824$), indicating that the model has clinical utility; the correlation coefficient of the external validation result r is 0.645, which further affirmed the stability of the model. At the same time, Bland-Altman analysis showed good agreement between the two. It suggests that this model can be used to clinically assess the difficulty of HIFU in treating uterine fibroids, provide a reference for HIFU dose placement, and improve the safety and efficacy of the treatment.

This study has several limitations. (1) Due to the sample size limitation, this study did not divide the dataset into training and internal validation groups. Although this is a common limitation in studies with small sample sizes, it may reduce the generalizability and robustness of the model. In future research, with a larger sample size, we plan to divide the dataset into training and internal validation groups to enhance the model's reliability. (2) HIFU ablation was performed by multiple physicians, and it is possible that differences in maneuvers and proficiency may have had some impact on the results. (3) This study was a retrospective analysis with a small sample size, which may have resulted in selection bias.

Conclusion

The combined model has improved predictive efficacy for EEF, which is clinically important for predicting the difficulty of HIFU treatment for uterine fibroids. However, due to sample size limitations, further validation of the model using larger datasets or by other research groups is needed to assess its generalizability and robustness. The combined model has optimal predictive efficacy for EEF, which is clinically important for predicting the difficulty of HIFU treatment for uterine fibroids.

Data availability

The data used to support the results of this study are available from the corresponding author.

Received: 18 June 2024; Accepted: 15 January 2025

Published online: 25 January 2025

References

1. Wang, W. W. & Wang, S. X. Interpretation of guidelines related to the diagnosis and treatment of uterine fibroids. *J. Practical Obstetrics Gynecol.* **38**, 101–103 (2022) ((in chinese)).
2. Chinese Expert Consensus on the Diagnosis and Treatment of Uterine Fibroids. Chinese Expert Consensus on the Diagnosis and Treatment of Uterine Fibroids. *Chinese Journal of Obstetrics and Gynecology* **52**, 793–800, (2017). <https://doi.org/10.3760/cma.j.issn.0529-567x.2017.12.001>
3. Haar, G. T. & Coussios, C. High intensity focused ultrasound: Physical principles and devices. *Int. J. Hyperth. Off. J. Eur. Soc. Hyperth. Oncol. North Am. Hyperth. Group* **23**, 89–104. <https://doi.org/10.1080/02656730601186138> (2007).
4. Chan, A. H., Fujimoto, V. Y., Moore, D. E., Martin, R. W. & Vaezy, S. An image-guided high intensity focused ultrasound device for uterine fibroids treatment. *Med. Phys.* **29**, 2611–2620. <https://doi.org/10.1118/1.1513990> (2002).
5. Zhang, C., Jacobson, H., Ngobese, Z. E. & Setzen, R. Efficacy and safety of ultrasound-guided high intensity focused ultrasound ablation of symptomatic uterine fibroids in Black women: a preliminary study. *BJOG Int. J. Obstetrics Gynaecol.* **124**(Suppl 3), 12–17. <https://doi.org/10.1111/1471-0528.14738> (2017).
6. Yi, G. F. et al. Influence factors of energy efficiency factors in high-intensity focused ultrasound ablation of solitary uterine leiomyoma. *China Interventional Imaging Therapeutics* **15**, 674–678. <https://doi.org/10.13929/j.1672-8475.201805017> (2018).
7. Liu, Z., Gong, C., Liu, Y. & Zhang, L. Establishment of a scoring system for predicting the difficulty level of high-intensity focused ultrasound ablation of uterine fibroids. *Int. J. Hyperth. Off. J. Eur. Soc. Hyperth. Oncol. North Am. Hyperth. Group* **34**, 77–86. <https://doi.org/10.1080/02656736.2017.1325015> (2018).
8. Xia, T. et al. MRI-based radiomics and deep learning in biological characteristics and prognosis of hepatocellular carcinoma: Opportunities and challenges. *J. Magnetic Resonance Imaging JMRI* **59**, 767–783. <https://doi.org/10.1002/jmri.28982> (2024).
9. Cheng, Y. et al. Development and validation of a radiomics model based on T2-weighted imaging for predicting the efficacy of high intensity focused ultrasound ablation in uterine fibroids. *Quantit. Imaging Med. Surg.* **14**, 1803–1819. <https://doi.org/10.21037/qims-23-916> (2024).
10. Qin, S., Jiang, Y., Wang, F., Tang, L. & Huang, X. Development and validation of a combined model based on dual-sequence MRI radiomics for predicting the efficacy of high-intensity focused ultrasound ablation for hysteroscopic myoma. *Int. J. Hyperth. Off. J. Eur. Soc. Hyperth. Oncol. North Am. Hyperth. Group* **40**, 2149862. <https://doi.org/10.1080/02656736.2022.2149862> (2023).
11. Fan, H. J. et al. Factors affecting effects of ultrasound guided high intensity focused ultrasound for single uterine fibroids: a retrospective analysis. *Int. J. Hyperth. Off. J. Eur. Soc. Hyperth. Oncol. North Am. Hyperth. Group* **35**, 534–540. <https://doi.org/10.1080/02656736.2018.1511837> (2018).
12. Wu, J. et al. uRP: An integrated research platform for one-stop analysis of medical images. *Front. Radiol.* **3**, 1153784. <https://doi.org/10.3389/fradi.2023.1153784> (2023).
13. Wei, C. A predictive study of uterine fibroid pathologic staging, HIFU ablation difficulty and immediate ablation rate based on conventional MRI and T2WI-imaging histology, Anhui Medical University, (2021). ((in chinese))
14. Lubner, M. G., Smith, A. D., Sandrasegaran, K., Sahani, D. V. & Pickhardt, P. J. CT Texture analysis: Definitions, applications, biologic correlates, and challenges. *Radiograph Rev Publication Radiol Soc North Am Inc* **37**, 1483–1503. <https://doi.org/10.1148/r.2017170056> (2017).
15. Miles, K. A., Ganesan, B. & Hayball, M. P. CT texture analysis using the filtration-histogram method: what do the measurements mean?. *Cancer Imaging Off. Publicat. Int. Cancer Imaging Soc.* **13**, 400–406. <https://doi.org/10.1102/1470-7330.2013.9045> (2013).
16. Yang, M. J., Yu, R. Q., Chen, W. Z., Chen, J. Y. & Wang, Z. B. A prediction of NPVR \geq 80% of ultrasound-guided high-intensity focused ultrasound ablation for uterine fibroids. *Front. Surg.* **8**, 663128. <https://doi.org/10.3389/fsurg.2021.663128> (2021).
17. Zhao, W. P., Chen, J. Y. & Chen, W. Z. Dynamic contrast-enhanced MRI serves as a predictor of HIFU treatment outcome for uterine fibroids with hyperintensity in T2-weighted images. *Exp. Therapeutic Med.* **11**, 328–334. <https://doi.org/10.3892/etm.2015.2879> (2016).
18. Zhao, W. P. *Study on the safety and effectiveness of ultrasound ablation of MRI-T2WI high-signal uterine fibroids* (Chongqing Medical University, 2013) ((in chinese)).
19. Hyvärinen, M., Huang, Y., David, E. & Hynynen, K. Comparison of computer simulations and clinical treatment results of magnetic resonance-guided focused ultrasound surgery (MRgFUS) of uterine fibroids. *Med. Phys.* **49**, 2101–2119. <https://doi.org/10.1002/mp.15263> (2022).

Author contributions

Q.Y. was responsible for guiding the study conception and design; X.H. and L.S. both contributed equally to the article and were mainly responsible for the study design, data collection and analysis, interpreting the results, and writing the manuscript; Y.Y.L. was responsible for the statistical analysis; S.W.B. was responsible for the data collection; and F.W. was responsible for the instruction of the software operation.

Declarations

Competing interests

The authors declare no competing interests.

Additional information

Supplementary Information The online version contains supplementary material available at <https://doi.org/10.1038/s41598-025-86958-0>.

Correspondence and requests for materials should be addressed to Q.Y.

Reprints and permissions information is available at www.nature.com/reprints.

Publisher's note Springer Nature remains neutral with regard to jurisdictional claims in published maps and institutional affiliations.

Open Access This article is licensed under a Creative Commons Attribution-NonCommercial-NoDerivatives 4.0 International License, which permits any non-commercial use, sharing, distribution and reproduction in any medium or format, as long as you give appropriate credit to the original author(s) and the source, provide a link to the Creative Commons licence, and indicate if you modified the licensed material. You do not have permission under this licence to share adapted material derived from this article or parts of it. The images or other third party material in this article are included in the article's Creative Commons licence, unless indicated otherwise in a credit line to the material. If material is not included in the article's Creative Commons licence and your intended use is not permitted by statutory regulation or exceeds the permitted use, you will need to obtain permission directly from the copyright holder. To view a copy of this licence, visit <http://creativecommons.org/licenses/by-nc-nd/4.0/>.

© The Author(s) 2025